

An Artificial Neural Network-Based Model Predictive Control for Three-phase Flying Capacitor Multi-Level Inverter

Abualkasim Bakeer^{1,*}, Ihab S. Mohamed^{2,*}, Parisa Boodaghi Malidarreh^{3,*}, Intissar Hattabi⁴, Lantao Liu²

Abstract—Model predictive control (MPC) has been used widely in power electronics due to its simple concept, fast dynamic response, and good reference tracking. However, it suffers from parametric uncertainties, since it directly relies on the mathematical model of the system to predict the optimal switching states to be used at the next sampling time. As a result, uncertain parameters lead to an ill-designed MPC. Thus, this paper offers a model-free control strategy on the basis of artificial neural networks (ANNs), for mitigating the effects of parameter mismatching while having a little negative impact on the inverter's performance. This method includes two related stages. First, MPC is used as an expert to control the studied converter in order to provide a dataset, while, in the second stage, the obtained dataset is utilized to train the proposed ANN. The case study herein is based on a four-level three-cell flying capacitor inverter. In this study, MATLAB/Simulink is used to simulate the performance of the proposed method, taking into account various operating conditions. Afterward, the simulation results are reported in comparison with the conventional MPC scheme, demonstrating the superior performance of the proposed control strategy in terms of robustness against parameters mismatch and low total harmonic distortion (THD), especially when changes occur in the system parameters, compared to the conventional MPC. **Furthermore, the experimental validation of the proposed method is provided based on the Hardware-in-the-Loop (HIL) simulation using the C2000TM-microcontroller-LaunchPadXL TMS320F28379D kit, demonstrating the applicability of the ANN-based control strategy to be implemented on a DSP controller.**

Index Terms—Model predictive control, Artificial neural network, Multilevel inverter, Total harmonics distortion, Hardware-in-the-Loop (HIL) simulation.

I. INTRODUCTION

POWER converters have been used in a wide range of applications in recent decades due to their improved performance and efficiency [1]. In this context,

¹ Abualkasim Bakeer is with the Department of Electrical Engineering, Faculty of Engineering, Aswan University, Aswan 81542, Egypt; abualkasim.bakeer@aswu.edu.eg

² Ihab S. Mohamed and Lantao Liu are with the Luddy School of Informatics, Computing, and Engineering, Indiana University, Bloomington, IN 47408 USA, {mohamedi, lantao}@iu.edu

³ Parisa Boodaghi Malidarreh is with the Department of Power Electronics and Electrical Machines, Iran University of Science and Technology (IUST), Iran, pboodaghi@gmail.com

⁴ Intissar Hattabi⁴ is with the Department of Automatic and Electrical Engineering, Saad Dahlab University of Science and Technology, BLIDA, Algeria hattabiintissar4@gmail.com

* Abualkasim Bakeer, Ihab S. Mohamed, and Parisa Boodaghi Malidarreh contributed equally to this work as the first author.

substantial attention has been paid to multilevel inverters (MLIs) that introduced with certain advantages, such as: (i) reducing the total harmonic distortion, (ii) reducing common-mode voltage, and (iii) reducing the dv/dt (that is, the rate of voltage change over time in switching instant) stress that leads to a reduction in electromagnetic emissions. There are a number of well-established and conventional MLI topologies that have been implemented and refined over time, such as: flying capacitor (FC), cascaded H-Bridge (CHB), neutral point clamped (NPC), as well as innovative topologies that combine different topologies to improve MLIs performance [2]. As a result, different control methods have been investigated including various linear methods such as proportional-integral (PI) with pulse width modulation (PWM) or space vector modulation (SVM) [3], [4], non-linear methods with Hysteresis [5], and other non-classical (i.e., modern) control methods such as different techniques of predictive control [5], [6]. However, controlling the MLIs with the high number of switches brings about dire problems in controlling algorithms and makes them more complex. Moreover, voltage imbalance among the MLI capacitors becomes an important concern in designing efficient control algorithms [7]–[10].

Model predictive control, among several control methods described, has appealing aspects that demonstrate its proper functioning. It provides a fast transient response, straightforward implementation, and non-linear constraints consideration [11]–[14]. Furthermore, the development of efficient microprocessors accounts for applying the MPC schemes widely in machine drive, grid-connected converters, and power supplies [15]–[18]. By explicitly utilizing the model of the system to be controlled, MPC selects, at each time step, the optimal switching state that minimizes a pre-defined cost function. However, it has a high *online* computational burden especially when multiple time-horizons are considered, as: (i) the cost function should be calculated for different possible switching states; (ii) the optimization yields the optimal control sequence (i.e., optimal switching states); (iii) the first optimal switching state is finally applied to the system in the next sampling time. Sequentially, it can be quite difficult to employ the MPC to control MLIs with numerous levels [19]–[22]. In addition, as previously mentioned, MPC directly uses the mathematical

model of the system, and thus the prediction accuracy is sensitive to the change in system parameters. As a result, it is susceptible to perform incorrectly as a result of parameter variations that may occur in the real system due to degradation and temperature effects [23].

To be more specific, some non-modeled variables, such as temperature and magnetic saturation, have impacts on the real system's parameters that are so-called modeling errors or errors in measurements; these effects can deteriorate the control performance. Therefore, various control techniques have been proposed for tackling and analyzing the effects of parametric uncertainties [24], [25]. On the other hand, since *MPC* possesses a nonlinear structure, these studies were carried out empirically by studying the behavior of *MPC* under different uncertainty conditions [25], the obtained results led to adjust the model parameters such as inductance to mitigate the effects of the parameter mismatch. Moreover, the negative effects of mismatches in load resistance were ignored [23], [26]. For instance, authors in [26] examined the impact of electrical parameters' variation in six-phase induction motor drive. It has been shown that the parameter of inductance can affect the performance of *MPC*, especially the stator and rotor leakage. While, in [23], the predictive control-based direct power control with an adaptive parameter identification technique is proposed to cope with the parameter uncertainty problem. In this method, the input resistance and inductance of the converter are estimated using the input current and voltage at each sampling time, without having extra sensors. Thus, the converter parameters are updated online to curb the effects of parameter uncertainty.

Furthermore, the use of data-based control approaches, such as *ANN*-based control methods, has increased in recent research, particularly in power electronics and motor drives [27], [28]. Just to name a few, in [29], an *ANN*-based *MPC* control strategy was introduced to improve the performance of a three-phase inverter with an output *LC* filter, with comparison to the conventional *MPC* scheme. While, in [22], a general *ANN-MPC* scheme is presented to tackle the computational challenge in adopting *MPC* in highly complex power converters. In [30], the authors proposed a data-based technique for calculating the voltages of capacitors in order to eliminate the need for system sensors. While, an *ANN*-based method is used in [31] to regulate the weighting factors in the cost function of *MPC*, which represents one of the research challenges in Model Predictive Control. Moreover, data-based control schemes are used in motor drives for estimating rotor speed, rotor flux, and torque in induction motors [32]–[34]. In [35], the authors applied *ANN* to calculate the dwell-time of the 3-phase 2*L*-*VSI*, which can improve the THD at a fixed-switching frequency operation.

This paper proposes an artificial neural network-based (*ANN*-based) control strategy for a three-phase four-level flying capacitor inverter. *MPC* has been used as a baseline control scheme for (i) collecting the data

required for training process, considering different operating conditions, and (ii) assessing our proposed control strategy. The main contributions of the proposed *ANN*-based control strategy can be summarized as follows:

- 1) It is an *End-to-End (E2E)* control scheme that generates directly the optimal switching states of the inverter, without the need for either the mathematical model of the inverter or a pre-defined cost function to be minimized at each time step.
- 2) It reduces the effects of the parameter mismatch problems as it offers a model-free control strategy based on *ANNs*.
- 3) The proposed technique exhibits low *THD* in the output current compared to the conventional *MPC*.
- 4) The *HIL* simulation is utilized to better assess the performance of the *ANN*-based control method compared with conventional *MPC*.
- 5) Moreover, the impact of the input features selection on the performance of the proposed control strategy is studied and evaluated. Note that points 4) and 5) have not been addressed in the originally proposed method in [29].
- 6) Finally, we provide an open repository of the dataset and simulation files to the community for further research activities.

This paper is organized as follows. In Section II, the flying capacitor multilevel inverter (*FCMLI*) and its mathematical model are briefly described, whereas the model predictive control strategy is explained in Section III. The *ANN*-based *MPC* control strategy proposed in this work for the *FCMLI* is presented in Section IV. Simulation results for both control strategies are given in Section V. In Section VI, the *HIL* simulation is utilized to show the efficiency of the proposed *ANN*-based control strategy in comparison with the *MPC* scheme. Finally, conclusions are given in Section VII.

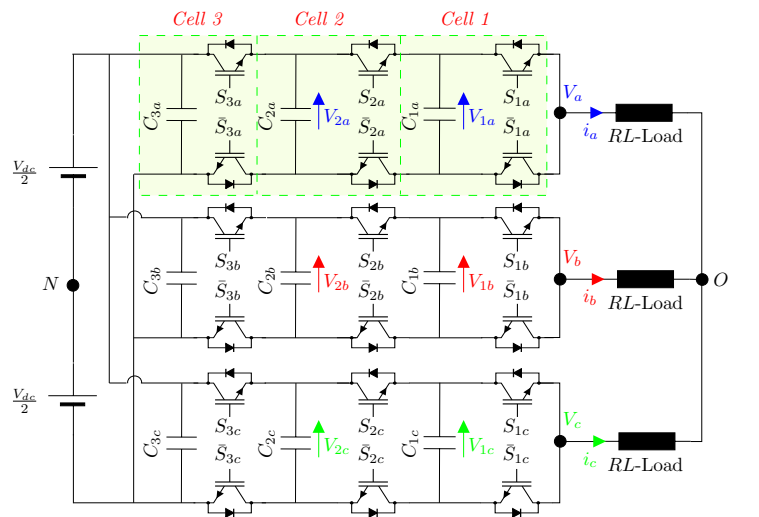


Fig. 1. Topology of a three-phase four-level flying capacitor inverter that is directly connected to an *RL*-load.

II. FLYING CAPACITOR MULTILEVEL INVERTER

Flying capacitor multilevel inverter (*FCMLI*) comprises series of connected cells which have a flying capacitor and two switches with antiparallel diodes. These switches are working in a complementary manner to avoid the short-circuit between the flying capacitor terminals. An N -cell *FCMLI* has $2N$ switches in each leg, and it produces $(N + 1)$ voltage levels from $\frac{-V_{dc}}{2}$ to $\frac{V_{dc}}{2}$, where V_{dc} denotes the input voltage source. The average voltage of each capacitor should be kept fixed at multiples of $\frac{V_{dc}}{N}$. The nearest capacitor to the load has $\frac{V_{dc}}{N}$, whilst the capacitor that is connected to the voltage source has V_{dc} ; the capacitor voltage ratio should be set as $V_{1x} : V_{2x} : V_{3x} = 1 : 2 : 3$ with $x \in \{a, b, c\}$ for generating the four-level voltage waveform. Fig. 1 shows a three-phase four-level flying capacitor (*FC*) inverter with three cells. Each capacitor's voltage can be estimated using the inverter current i_x and switching states in the corresponding leg, as given in (1) and (2). As it can be seen in Fig. 1, the third capacitor C_{3x} is in parallel with the input voltage source V_{dc} ; thus, V_{3x} is equal to V_{dc} . In addition, for a resistive-inductive load (i.e., RL -load), the three-phase output voltage can be written as in (3), where R and L are the load resistance and inductance, respectively. Table I displays the eight possible switching states of a single-phase *FCMLI* and the corresponding output voltage.

$$V_{1x} = V_{1x}(0) + \frac{1}{C_{1x}} \int_0^t i_x(S_{2x} - S_{1x}) dt \quad (1)$$

$$V_{2x} = V_{2x}(0) + \frac{1}{C_{2x}} \int_0^t i_x(S_{3x} - S_{2x}) dt \quad (2)$$

$$V_{xN} = Ri_x + L \frac{di_x}{dt} + \frac{1}{3}(V_{aN} + V_{bN} + V_{cN}) \quad (3)$$

Table I
SWITCHING STATES FOR A SINGLE-PHASE *FC* CONVERTER.

V_i	S_{1x}	S_{2x}	S_{3x}	Output voltage V_{xN}	Equation
V_0	0	0	0	$-V_{dc}/2$	$-V_{dc}/2$
V_1	1	0	0	$-V_{dc}/6$	$V_{1x} - V_{dc}/2$
V_2	0	1	0	$-V_{dc}/6$	$V_{2x} - V_{1x} - V_{dc}/2$
V_3	1	1	0	$V_{dc}/6$	$V_{2x} - V_{dc}/2$
V_4	0	0	1	$-V_{dc}/6$	$V_{dc}/2 - V_{2x}$
V_5	1	0	1	$V_{dc}/6$	$V_{dc}/2 - V_{2x} + V_{1x}$
V_6	0	1	1	$V_{dc}/6$	$V_{dc}/2 - V_{1x}$
V_7	1	1	1	$V_{dc}/2$	$V_{dc}/2$

III. MODEL PREDICTIVE CONTROL FOR *FCMLI*

Model predictive control (*MPC*) is one of the well-established and promising model-based control methods that is successfully used in power electronics. The key idea behind *MPC* is the use of the system model for predicting the future behavior of the variables to be controlled, considering a certain time horizon. To do so, it needs, in our case, the discrete model of the converter.

The optimal control signal, i.e., switching states as described in Table I, that minimizes the cost function is then determined. The entire *MPC* procedure for *FCMLI* is shown in Fig. 2, which can be described step-by-step as follows:

- 1) At sampling instant k , the controlled variables (namely, $V_{1x}^k, V_{2x}^k, i_x^k$) should be measured.
- 2) Those controlled variables are then predicted at instant $k + 1$ based on the discrete model of the converter given in (4) and (5), where $M_1 = \frac{T_s}{C_{1x}}$, $M_2 = 1 - \frac{RT_s}{L}$, and T_s is sampling time; while $V_{1x}^{k+1}, V_{2x}^{k+1}, i_x^{k+1}$ are the flying capacitor voltages and output current at instant $k + 1$.

$$V_{1x}^{k+1} = V_{1x}^k + \frac{T_s}{C_{1x}} i_x^k (S_{2x}^i - S_{1x}^i) \quad (4)$$

$$V_{2x}^{k+1} = V_{2x}^k + \frac{T_s}{C_{2x}} i_x^k (S_{3x}^i - S_{2x}^i) \quad (5)$$

$$i_x^{k+1} = (V_{xN} - V_{ON}) M_1 + i_x^k M_2 \quad (6)$$

where V_{ON} is the common mode voltage.

- 3) After defining a proper cost function J_i , as in (6), it should be calculated for the current switching states S_i based on the desired value of each controlled variable, namely, $V_{1x}^*, V_{2x}^*, i_x^*$.
- 4) As the main objective of the optimization problem is to find the optimum switching state (S_{opt}) that minimizes the cost function, the cost function of the current switching state J_i is compared with the smallest previous value e .
- 5) Steps 2) to 4) are repeated for all possible switching states given in Table I.
- 6) Finally, the optimum switching state (S_{opt}) is applied at the next sampling instant.

In Fig. 2, N refers to the total number of the possible switching states in each phase, which is equal to 8 in this study.

One of the most critical stages of *MPC*, as previously stated, is determining the optimal switching state (S_{opt}) that minimizes a given cost function. Different forms of cost functions have been established, in this regard, which are used according to the requirements from the *MPC* design. In this work, the cost function is expressed as (6), where i_x^* and i_x^{k+1} are the reference and estimated values of the output current at $k + 1$, respectively. Similarly, $V_{1x}^{k+1}, V_{2x}^{k+1}$ and V_{1x}^*, V_{2x}^* refer to the first and second capacitor voltages and their desired values at $k + 1$, respectively. λ_1 and λ_2 are weighting factors of the cost function that determines the importance of the related term in the cost function. For instance, a higher weighting factor indicates the importance of the variable in determining the optimal switching state, thus it shows the priority of that variable in determining the optimal switching state. As previously described, the cost function must be evaluated for all switching states

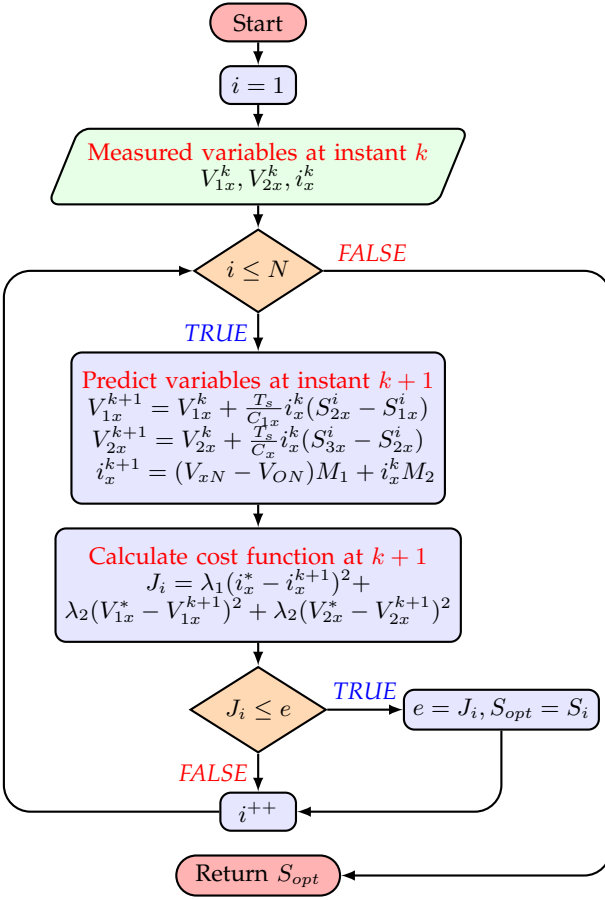


Fig. 2. Flowchart diagram of MPC scheme for FCMLI.

at each sampling time, which can be difficult in systems with many possible switching states such as multilevel inverters; thereby, it needs a strong microprocessor to deal with this high computational burden. In fact, the major drawback of MPC is its optimization procedure that should be solved online, which imposes a large amount of *real-time* calculation. This is an important motivation for proposing an *End-to-End* (E2E) control strategy, such as ANN-Based control strategy, that generates directly the optimal switching states of the inverter, without the need for either: (i) the mathematical model of the inverter and (ii) a pre-defined cost function to be minimized [29].

IV. PROPOSED ANN-BASED CONTROL STRATEGY

This section provides a brief overview of the artificial neural network (ANN) followed by a detailed explanation of the proposed ANN-based control strategy for controlling the FCMLI. Moreover, it studies the influence of considering different input features on the performance of the ANN-based control scheme.

A. Overview of ANN

Artificial neural network (ANN) is a subset of machine learning that can be directly defined as a mathematical

relationship between input features and targets; in other words, it is a mathematical model that uses learning algorithms to make intelligent decisions based on historical data. It consists of a set of nodes, so-called neurons, that form layers that are connected and executed in parallel. Fig. 3 shows the typical architecture of a multi-

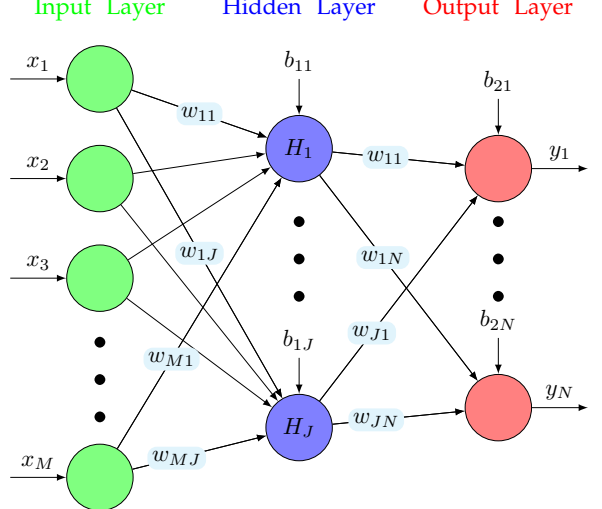


Fig. 3. A typical architecture of a two-layer ANN with M inputs, one hidden layer containing J neurons, and N outputs.

input multi-output ANN that has M input features (i.e., $x_m \forall m = \{1, \dots, M\}$) and yields N output targets (namely, $y_n \forall n = \{1, \dots, N\}$), where the number of neurons in both input and output layers should be equivalent to the number of data to be processed and the number of targets, respectively. Each input feature x_m is multiplied by weighting factors $w_{mj} \forall j = \{1, \dots, J\}$ and applied to the hidden layer. In the hidden layer, the bias b_{1j} is added to the sum of the weighted values and an activation function is applied to it in each neuron; then, the results are multiplied by another weighting factors w_{jn} before being passed to the output layer. Those correction factors (i.e., biases) allow us to shift the activation functions, which improves the model's fit to the given dataset. The mathematical formulation of the n^{th} output can be described as:

$$y_n = h \left(\sum_{j=1}^J w_{jn} H_j + b_{2n} \right), \quad \forall n = \{1, \dots, N\}, \quad (7)$$

$$H_j = h \left(\sum_{m=1}^M w_{mj} x_m + b_{1j} \right), \quad \forall j = \{1, \dots, J\},$$

where h is the activation function, H_j are the outputs of the hidden layer, and b_{2n} refer to the biases of the output layer. Activation functions h (such as *sigmoid*, *hyperbolic tangent*, *softmax*, and *linear*) are the key part of the neural network design that are used to learn complicated patterns and assess how well the network model learns the training dataset [36]. Moreover, there exist different learning methods; in this study, the feed-forward method

is used. Unlike recurrent neural networks, connections between different nodes in various layers do not produce a cycle in the feed-forward learning approach.

B. ANN-Based Control Strategy

The *ANN*-based control scheme proposed, in this work, undergoes two main phases, namely, training and testing phases. As mentioned above, the *ANN* should be first trained *offline*. To do so, *MPC* has been used as a baseline control scheme for assessing our proposed control strategy and, in the meanwhile, for collecting data required for training, validation, and testing the proposed neural network. The acquired *MPC* dataset is used to train the *ANN* to anticipate the optimal switching state S_{opt} at the instant $k + 1$. Afterwards, once the proposed neural network is fine-tuned, it can be successfully used *online* for controlling the *FCMLI*, instead of relying on the predictive control strategies.

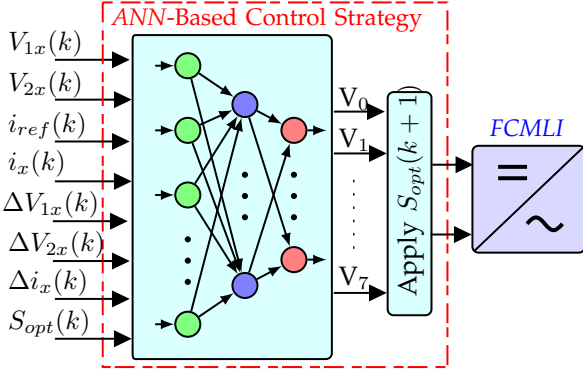


Fig. 4. Block diagram of the *ANN*-based control strategy, considering $\mathbf{X}_2 = \{V_{1x}, V_{2x}, i_{ref}, i_x, \Delta V_{1x}, \Delta V_{2x}, 2\Delta i_x, S_{opt}\}$ as input features.

In this study, the input features of our proposed *ANN*-based control scheme consist of a set of measured variables of the inverter **that will be discussed in Section IV-C**, while the output includes the optimal switching states S_{opt} that should be applied to the inverter at next sampling instant $k + 1$, as illustrated in Fig. 4. More precisely, the output includes a vector of eight elements that identifies the eight voltage vectors ($V_i \forall i \in \{0, \dots, 7\}$) (see Table I). Each sampling instant, the index of the *optimum* voltage vector will be only active with a value of one, whereas others will be equal to zero.

C. Input Features Selection and Training Process

Basically, selecting the best set of input features is a significant part of designing the *ANN*-based control strategy. Based on the type of inverters and the main purpose of the study, different features can become efficient in both the training phase and testing phase that assess the capability of learning the mathematical model of the system to be controlled and its dynamics. **For the *FCMLI*, the input features are considered to be a combination of**

measured variables such as capacitor's voltage, output current and voltage, switching states, and current errors. We have **empirically** observed that in order to seek the best mapping from the raw input data to the desired outputs, different combinations of input features should be first considered and then assessed. **Furthermore, it is observed that adding the optimal switching state S_{opt} at instant k to the input features improves the performance of the learning-based control strategy.**

To be more specific, five different sets of input features, named: \mathbf{X}_1 , \mathbf{X}_2 , \mathbf{X}_3 , \mathbf{X}_4 , and \mathbf{X}_5 , are chosen and then assessed, as illustrated in Table II. It can be seen, for instance, that \mathbf{X}_1 is composed of 9 measurable variables, namely: $\{V_{1x}, V_{2x}, i_{ref}, i_x, \Delta V_{1x}, \Delta V_{2x}, \Delta i_x, S_{opt}, V_{ph}\}$, where $\Delta V_{1x} = (\frac{V_{dc}}{3} - V_{1x})$, $\Delta V_{2x} = (\frac{2V_{dc}}{3} - V_{2x})$, $\Delta i_x = (i_{ref} - i_x)$, S_{opt} is the optimal switching state at time instant k , and V_{ph} refers to the four-level output voltage. To evaluate each input set $\mathbf{X}_i \forall i \in \{1, 2, \dots, 5\}$, a set of training samples (i.e., S_1, S_2, \dots, S_{16}) that represent different operating conditions are considered. Each sample has different system parameters such as input voltage V_{dc} , sampling time T_s , *RL* impedance, and reference output current i_{ref} (see Table II). Afterward, these samples that have been acquired by *MPC* provide a new dataset, which is then used to train the *ANN* for each \mathbf{X}_i . In the following, the inverter is directly controlled using trained *ANN* with each of the \mathbf{X}_i and the *THD* of the output current i_x is computed. This procedure repeats for each \mathbf{X}_i and the results of different operating conditions (i.e., for sample $S_i \forall i \in \{1, 2, \dots, 16\}$) are reported in Table II. In fact, the *THD* of the output current i_x is used as a decision parameter to find the best set of input features \mathbf{X}_i to be used in the next sections. We can observe from the preliminary results given in Table II that the performance of the proposed control strategy on the basis of \mathbf{X}_5 , in which the lowest set of features is used, is the worst as the *THD* is quite higher. Furthermore, it can be observed that the four-level output voltage V_{ph} that has been added to \mathbf{X}_1 , does not have much improvement. For that reason, \mathbf{X}_2 is selected as input features for the proposed control scheme given in Fig. 4, due to its significant improvement compared to other considered sets. \mathbf{X}_2 is composed of 8 measurable variables, namely: $\{V_{1x}, V_{2x}, i_{ref}, i_x, \Delta V_{1x}, \Delta V_{2x}, 2\Delta i_x, S_{opt}\}$.

Once the effective set of features is selected, *MPC* is again utilized for providing the required dataset for training the proposed control scheme given in Fig. 4. Similar to Table II, various training samples (namely, S_1, S_2, \dots, S_{11}) have been acquired by *MPC*, each comprising different system parameters that were previously defined in Table II (namely, $V_{dc}, R, L, T_s, i_{ref}$) in addition to different values of the cell capacitance C . The eleven different samples are defined as a percentage of the nominal values of the converter parameters which are as follows: $V_{dc} = 360$ V, $C = 680$ μ F, $L = 10$ mH, $R = 15$ Ω , $i_{ref} = 15$ A, while the *MPC*'s sampling time T_s is indicated in the last column. For instance, S_1 is applied to the *FC* inverter and acquired, considering

Table II

THD OF THE OUTPUT CURRENT i_x FOR DIFFERENT SETS OF INPUT FEATURES, WHERE THE LOWEST THD IS HIGHLIGHTED IN BLUE.

Sample No.	S_1	S_2	S_3	S_4	S_5	S_6	S_7	S_8	S_9	S_{10}	S_{11}	S_{12}	S_{13}	S_{14}	S_{15}	S_{16}
V_{dc} [V]	360	360	360	342	378	360	360	350	340	360	340	350	360	350	350	350
T_s [μs]	30	30	30	20	20	45	45	50	50	20	25	20	20	25	40	
R [Ω]	10	15	25	7.5	15	15	8	9	11	10	10	12	7	9	9	
L [mH]	5	10	12	8	4.5	9	10	9.5	5	5.5	5	5	7	5	5	
i_{ref} [A]	17	12	5	12	10	4	5	6	4.35	12	10	8	15	12	12	
$\mathbf{X}_1 = \{V_{1x}, V_{2x}, i_{ref}, i_x, \Delta V_{1x}, \Delta V_{2x}, \Delta i_x, S_{opt}, V_{ph}\}$																
THD [%]	1.89	1.29	3.09	1.30	2.02	4.54	3.51	3.22	6.48	8.88	1.44	2.01	1.85	1.40	1.73	2.68
$\mathbf{X}_2 = \{V_{1x}, V_{2x}, i_{ref}, i_x, \Delta V_{1x}, \Delta V_{2x}, 2\Delta i_x, S_{opt}\}$																
THD [%]	1.65	1.06	2.36	0.93	2.07	4.13	3.73	3.17	6.22	8.01	1.41	2.21	1.25	1.20	1.69	3.06
$\mathbf{X}_3 = \{V_{1x}, V_{2x}, i_{ref}, i_x, \Delta V_{1x}, \Delta V_{2x}, \Delta i_x, S_{opt}\}$																
THD [%]	1.90	1.32	3.28	1.36	1.94	4.38	3.78	3.37	6.29	8.11	1.47	1.98	1.43	1.22	1.74	2.69
$\mathbf{X}_4 = \{V_{2x}, i_{ref}, i_x, \Delta V_{1x}, \Delta V_{2x}, \Delta i_x, S_{opt}\}$																
THD [%]	1.59	1.31	3.64	1.08	2.08	4.39	3.53	3.22	6.57	7.98	1.43	2.03	1.71	1.74	1.69	2.67
$\mathbf{X}_5 = \{i_{ref}, i_x, \Delta V_{1x}, \Delta V_{2x}, \Delta i_x, S_{opt}\}$																
THD [%]	2.69	1.45	3.53	1.32	2.04	4.55	3.71	3.50	6.62	8.11	1.81	2.11	1.65	1.76	1.99	2.94

$V_{dc} = 342$ V (i.e., 95% of its nominal value), $C = 646$ μ F, $L = 10$ mH, $R = 12$ Ω, $i_{ref} = 14.39$ A, and $T_s = 30$ μs.

Output Class	Target Class															
	1	2	3	4	5	6	7	8	9	10	11	12	13	14	15	16
1	21347 13.6%	0 0.0%	235 0.1%	340 0.2%	254 0.2%	0 0.0%	0 0.0%	0 0.0%	96.3% 3.7%							
2	0 0.0%	21459 13.6%	0 0.0%	0 0.0%	0 0.0%	300 0.2%	284 0.2%	298 0.2%	96.1% 3.9%							
3	358 0.2%	0 0.0%	16889 10.7%	732 0.5%	890 0.6%	324 0.2%	137 0.1%	30 0.0%	87.2% 12.8%							
4	258 0.2%	0 0.0%	963 0.6%	15247 9.7%	760 0.5%	141 0.1%	8 0.0%	85 0.1%	87.3% 12.7%							
5	297 0.2%	0 0.0%	951 0.6%	856 0.5%	17172 10.9%	8 0.0%	130 0.1%	253 0.2%	87.3% 12.7%							
6	0 0.0%	272 0.2%	206 0.1%	121 0.1%	5 0.0%	16963 10.8%	680 0.4%	940 0.6%	88.4% 11.6%							
7	0 0.0%	254 0.2%	169 0.1%	0 0.0%	125 0.1%	911 0.6%	15415 9.8%	843 0.5%	87.0% 13.0%							
8	0 0.0%	285 0.2%	14 0.0%	151 0.1%	359 0.2%	912 0.6%	888 0.6%	16981 10.8%	86.7% 13.3%							
	95.9% 4.1%	96.4% 3.6%	86.9% 13.1%	87.4% 12.6%	87.8% 12.2%	86.7% 13.3%	87.9% 12.1%	87.4% 12.6%	89.8% 10.2%							

Fig. 5. Training confusion matrix for 70% a training set with a misclassification error of 10.2%, where the number of correctly and incorrectly classified observations are shown in green and red, respectively.

In this work, the total dataset is randomly divided into three sets: training set, validation set, and testing set with 70%, 15%, and 15% of the total dataset, respectively. The optimum number of hidden layers is determined by varying the number of hidden layers and observing the testing accuracy. In addition, the *trainscg* function is used as a training function. After the training process, the trained ANN can be used to control the four-level three-phase flying capacitor inverter. The training confusion matrix that assesses the performance of the

training is shown in Fig. 5, where the lowest validation error is 0.1016 taken from epoch 701 and the overall accuracy is 89.80% with the total instances numbers of 509,788. The training results are summarized in Table IV, demonstrating that the training dataset based on \mathbf{X}_2 is properly selected, resulting in an efficient control system.

Table III
TRAINING SAMPLES OF THE ANN-BASED CONTROL STRATEGY.

Sample No.	$V_{dc} = 360$ [V]	$C = 680$ [μ F]	$L = 10$ [mH]	$R = 15$ [Ω]	$i_{ref} = 15$ [A]	T_s [μs]
S_1	0.95	0.95	1.00	0.80	0.95	30
S_2	0.90	0.85	0.95	0.70	0.90	10
S_3	1.25	0.90	1.20	1.10	1.15	50
S_4	1.10	1.05	1.50	1.23	1.05	60
S_5	1.00	1.10	1.05	1.40	0.75	15
S_6	1.00	0.98	0.75	1.30	0.65	18
S_7	1.15	1.20	0.80	1.17	0.55	50
S_8	1.00	1.07	0.88	0.77	0.85	30
S_9	1.00	1.00	0.98	0.87	0.50	40
S_{10}	1.00	1.00	0.90	0.10	2.00	5
S_{11}	1.00	1.00	0.90	0.10	2.00	15

Table IV
TRAINING RESULTS.

No. instances	Accuracy	Error (Epoch)
509,788	89.80%	0.1016 (701)

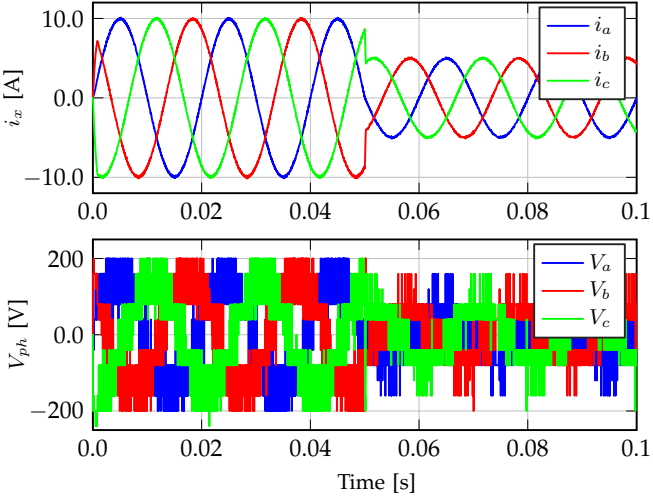


Fig. 6. Dynamic response of ANN-based control strategy: Output current and voltage when the reference current i_{ref} changes from $i_{ref} = 10$ A to $i_{ref} = 5$ A at $t = 0.05$ s.

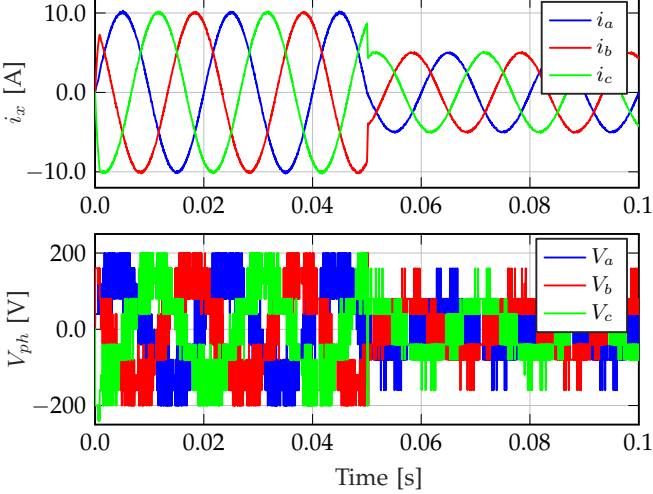


Fig. 7. Dynamic response of MPC: output current and voltage when the reference current i_{ref} changes from $i_{ref} = 10$ A to $i_{ref} = 5$ A at $t = 0.05$ s.

V. SIMULATION RESULTS AND DISCUSSION

In this section, the ANN-based control strategy is simulated using MATLAB/Simulink software and its performance is compared to that of the conventional MPC. The parameters of the FCMLI given in Fig. 1 are listed in Table V.

The dynamic behavior of the ANN-based and MPC control schemes are illustrated in Figs. 6 and 7, respectively. Both figures show the output current i_x and four-level output voltage V_{ph} under a sudden change of reference current i_{ref} from 10 A to 5 A at $t = 0.05$ s. It is observed that both methods have similar and good performance under dynamic conditions, since both control strategies track the reference current properly. The behavior of our proposed ANN-based control strategy under steady-state condition is depicted in Fig. 8, while

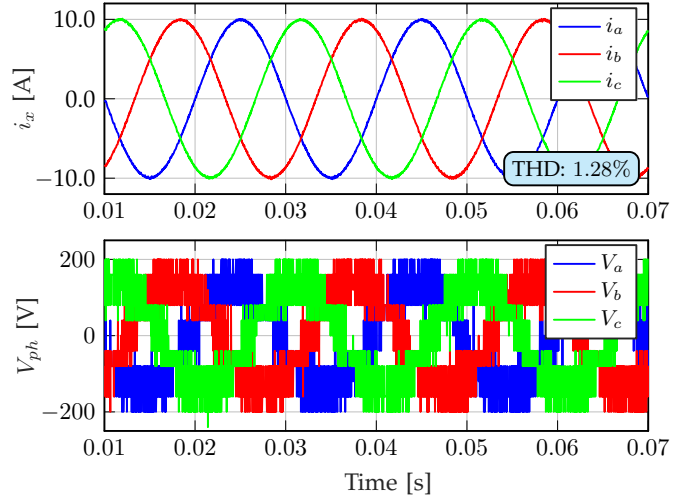


Fig. 8. Simulation results of ANN-based control strategy: Output current and four-level voltage.

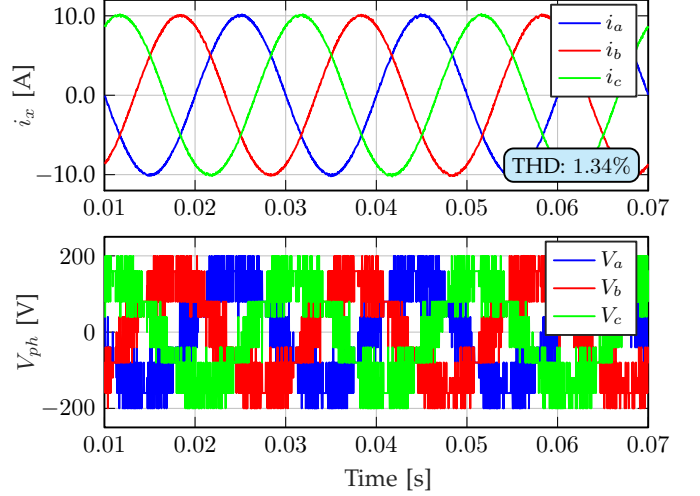


Fig. 9. Simulation results of MPC: Output current and four-level voltage.

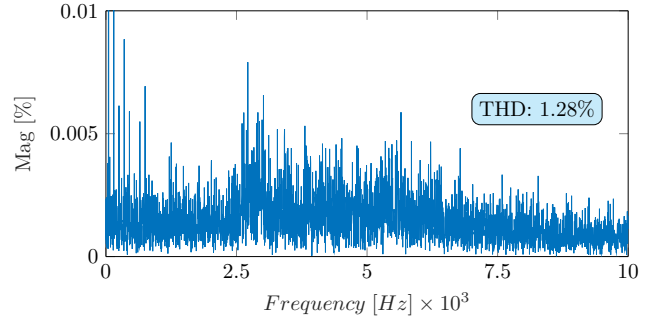


Fig. 10. Frequency spectrum of output current for the ANN-based control strategy.

the behavior of the classical MPC is shown in Fig. 9. It can be seen in the figures that the two control strategies generate a high-quality sinusoidal output current i_x with low distortion. However, the THD of the output current

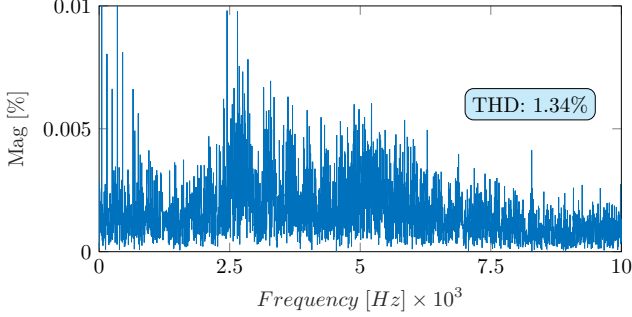


Fig. 11. Frequency spectrum of output current for the MPC scheme.

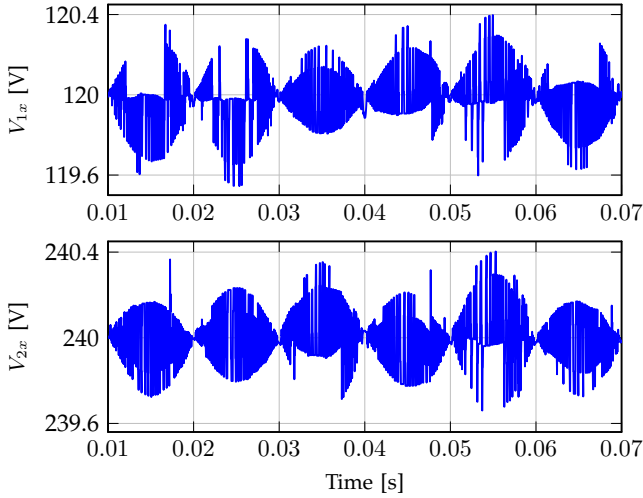


Fig. 12. Simulation results of ANN-based control strategy: Voltages of the capacitors.

in the case of an ANN-based control scheme is slightly lower than that in the case of MPC, namely, 1.34% compared to 1.28% in case of ANN-based method. For more information, the frequency spectrum of the two control methods are shown in Figs. 10 and 11. In addition, the voltages of the capacitors (i.e., V_{1x} , V_{2x}) obtained by the two proposed control strategies are depicted in Figs. 12 and 13, respectively. As can be observed, our proposed control scheme has a proper performance to keep the voltage at its desired value, as well as the MPC scheme.

As previously described, the ANN-based control strategy can be used to deal with the parameter uncertainty issues that arise in real systems. Thus, to verify the efficiency of the ANN-based MPC technique in this scope, another simulation study is carried out, where both control strategies are utilized to compare their performance under this condition. More precisely, the load inductance L is changed from 10 mH to 5 mH at $t = 0.1$ s; the obtained results are depicted in Figs. 14 and 15. By comparison between these two figures, it can be seen that the proposed ANN-based control scheme has better performance in such a situation. This can be clearly seen in the THD of the output current for the ANN-based control scheme that has a 2.78% compared to

Table V
PARAMETERS OF THE FCMLI.

Parameter	Value
R	15 [Ω]
L	10 [mH]
C	680 [μF]
V_{dc}	360 [V]
T_s	30 [μs]
f	50 [Hz]

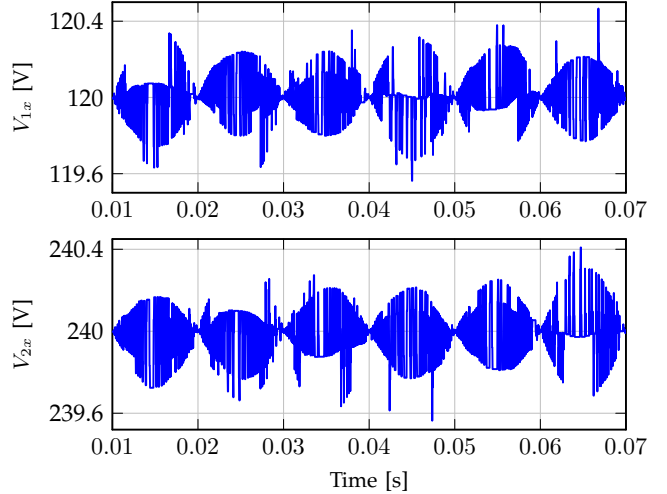


Fig. 13. Simulation results of MPC: Voltages of the capacitors.

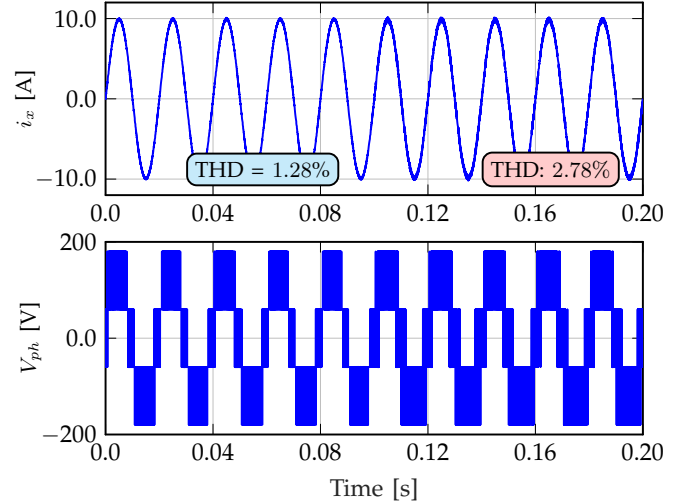


Fig. 14. Performance of our proposed ANN-based control strategy under load inductance variation from $L = 10$ mH to $L = 5$ mH at $t = 0.1$ s.

3.05% in the case of MPC after changing the inductance value, which demonstrates that the proposed control scheme is more robust to the parameter uncertainty than the classical MPC.

To better assess and show the superiority of the proposed control strategy in learning the mathematical model of the inverter and its dynamics, a comparison

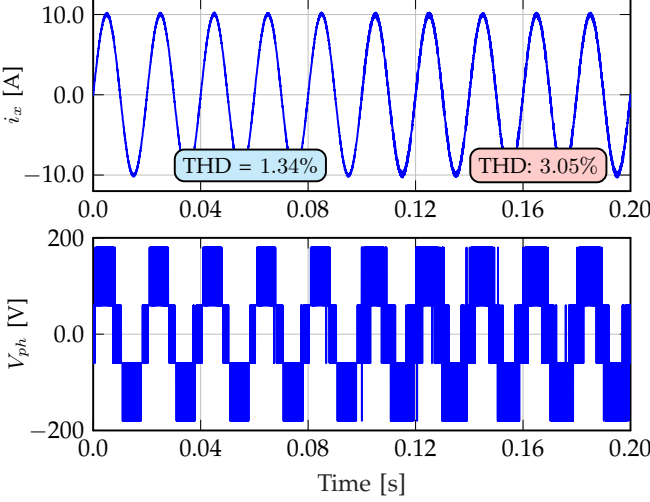


Fig. 15. Performance of the *MPC* scheme under load inductance variation from $L = 10\text{ mH}$ to $L = 5\text{ mH}$ at $t = 0.1\text{ s}$.

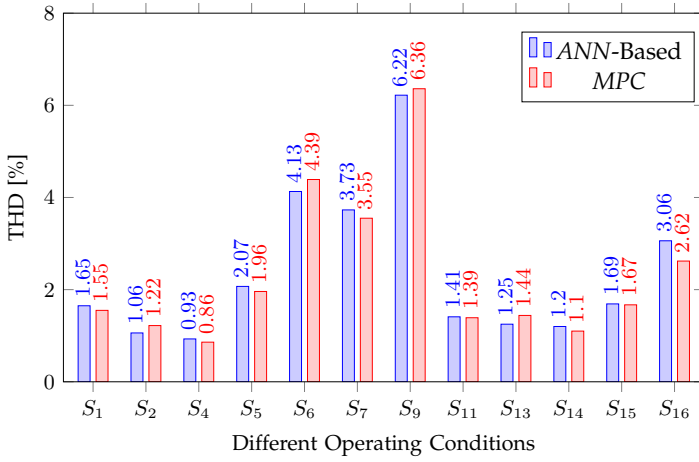


Fig. 16. THD comparison of output current between *MPC* and *ANN*-based control strategy.

of the *THD* of the output current obtained by the two control strategies is represented in Fig. 16, considering the different operating conditions listed in Table II. The obtained results demonstrate that the proposed *ANN*-based control scheme on the basis of the selected input feature (namely, X_2) has good performance compared to the conventional *MPC*, without requiring a large amount of training data.

VI. EXPERIMENTAL VALIDATION AND RESULTS

In this section, a rapid prototyping technique was utilized to implement the proposed *ANN*-based control strategy that previously described in Section IV. More precisely, a Hardware-in-the-Loop (HIL) simulator was used to verify and validate our proposed control scheme for controlling a three-phase four-level flying capacitor inverter.

Figure 17 illustrates the basic components and signal flows of the HIL simulation for the proposed

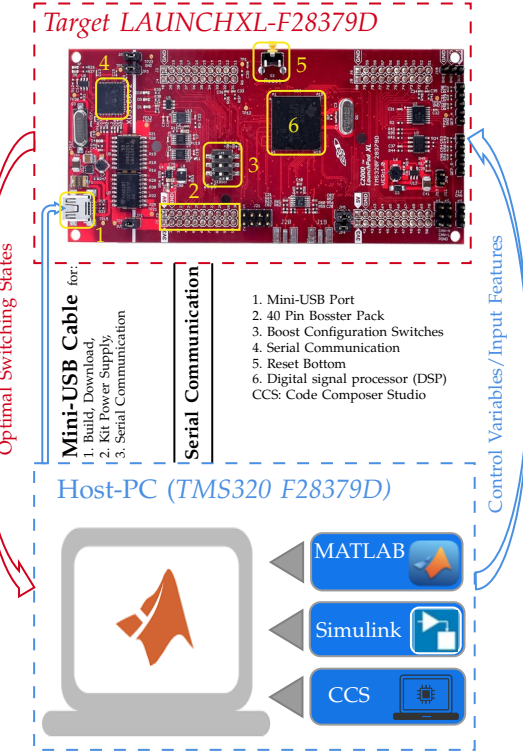


Figure 17. Schematic diagram of the HIL simulation for the proposed system, with the main components and signals flow.

system. For a typical HIL simulation, the control strategies (namely, *MPC* and *ANN*-based) are implemented in an external target micro-controller kit (in our study, C2000TM-microcontroller-LaunchPadXL TMS320F28379D kit), while the three-phase four-level flying capacitor inverter and its different loads are simulated and hosted on the personal computer (i.e., Host-PC) as a model in the MATLAB. The HIL simulation requires cooperation between the Host-PC and the Target LAUNCHXL-F28379D, which is achieved using a virtual serial COM port [37]. To be more specific, the Host-PC transmits the measured signals (or, input features) such as V_{1x} , V_{2x} , i_{ref} , i_x , ΔV_{1x} , ΔV_{2x} , Δi_x to the LAUNCHXL-F28379D kit. Afterwards, once the target kit receives these signals, the proposed control strategy selects the optimal switching state S_{opt} to be applied in the next sampling instant. Finally, the Host-PC receives S_{opt} to feed the inverter switches. This procedure will be repeated every sampling time T_s . More details about the HIL design procedures, including the simulation setup, Code Composer Studio (CCS), installation, building the target model, and running the Host program, can be found in [38].

After setting up the hardware and the Host-PC as described in [38], the HIL simulation is used to assess the performance of the proposed control schemes in controlling the output current i_x , phase voltage V_{ph} and voltage of the capacitors V_{1x} and V_{2x} . Figures 18 and 19 show the voltages of the capacitors for each control method. It can be seen that both *ANN*-based and *MPC* have the same

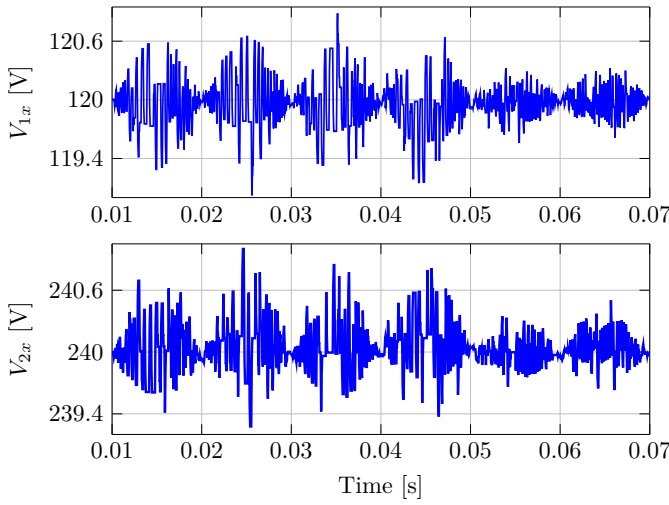


Fig. 18. HIL results of ANN-based control strategy: Voltages of the capacitors.

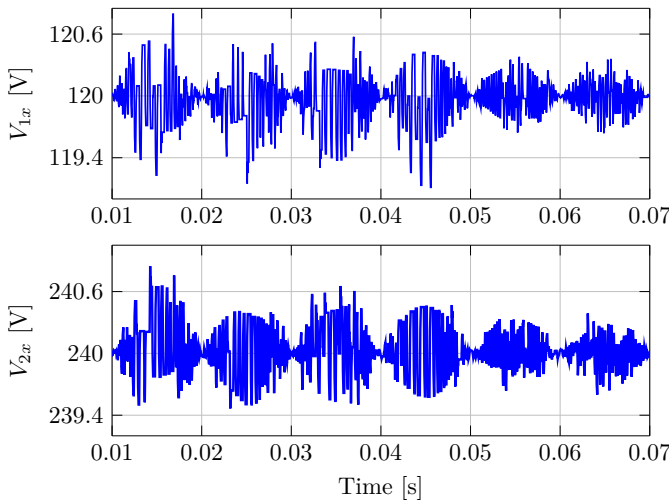


Fig. 19. HIL results of MPC scheme: Voltages of the capacitors.

and qualified performance to keep the voltage at the desired values, as previously depicted in the simulation section (see Figs. 12 and 13). In Figs. 20 and 21, we validate the performance of the two control strategies to deal with the parameter uncertainty problem, which is clearly described and tested in the previous section (see Figs. 14 and 15). It can be seen in Figs. 20 and 21 that after changing the inductance from $L = 10 \text{ mH}$ to $L = 5 \text{ mH}$ at $t = 0.1 \text{ s}$, the ANN-based control strategy has better performance in comparison with the classical MPC scheme. This comparison is carried out based on the THD of the output current which is 6.13% for the proposed control method, after changing the inductance value, compared to 8.70% when the MPC is employed. These results demonstrate the applicability and good performance of our proposed control strategy under realistic conditions.

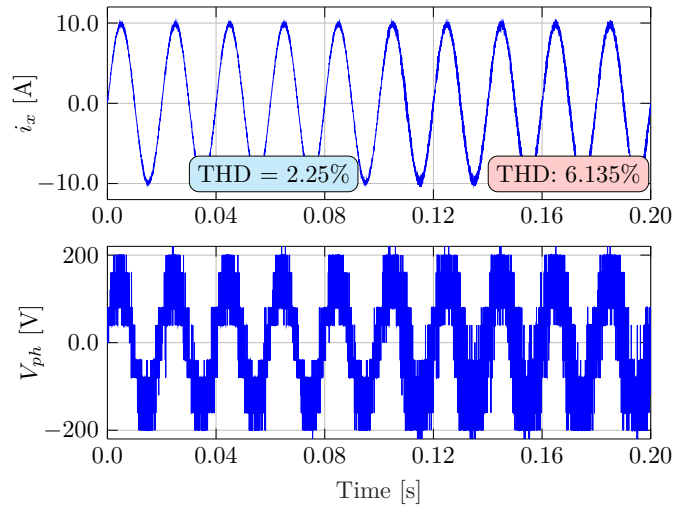


Fig. 20. HIL results: Performance of the ANN-based control scheme under load inductance variation from $L = 10 \text{ mH}$ to $L = 5 \text{ mH}$ at $t = 0.1 \text{ s}$.

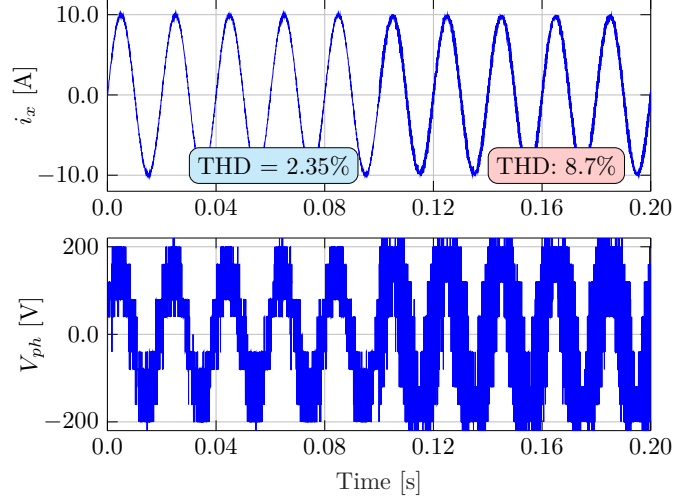


Fig. 21. HIL results: Performance of the MPC scheme under load inductance variation from $L = 10 \text{ mH}$ to $L = 5 \text{ mH}$ at $t = 0.1 \text{ s}$.

VII. CONCLUSIONS

In this paper, we have proposed an ANN-based control strategy for controlling a three-phase four-level flying capacitor inverter with the aim of generating a high-quality sinusoidal output current and improving the robustness against parametric mismatches, especially when compared to conventional MPC scheme. The proposed control scheme employs the classical MPC to generate a reliable dataset of inverter variables to be used as input features by the proposed a feed-forward ANN. Afterwards, once the *off-line* training is performed based on the obtained data from MPC, it can be used to directly control the inverter without the requirement for a mathematical model of the system. Simulation results reveal that ANN-based control strategy performs better with respect to the THD under most conditions. Additionally, an experiment is carried out for assessing

its robustness against parameter uncertainty. Moreover, to better assess the performance of the proposed ANN-based control method compared to the traditional MPC, HIL simulation is utilized to demonstrate its applicability to be run on a DSP kit and prove its efficiency under parameter mismatch problems. According to the results, the proposed control scheme showed better performance than the conventional MPC under parameter mismatch conditions, owing to the fact that, unlike MPC, the proposed technique does not depend on the system model.

REFERENCES

- [1] P. Cortés, G. Ortiz, J. I. Yuz, J. Rodríguez, S. Vazquez, and L. G. Franquelo, "Model predictive control of an inverter with output LC filter for UPS applications," *IEEE Transactions on industrial electronics*, vol. 56, no. 6, pp. 1875–1883, 2009.
- [2] T. G. Habetler, R. Naik, and T. A. Nondahl, "Design and implementation of an inverter output LC filter used for dv/dt reduction," *IEEE Transactions on Power Electronics*, vol. 17, no. 3, pp. 327–331, 2002.
- [3] J. Jung, M. Dai, and A. Keyhani, "Optimal control of three-phase pwm inverter for ups systems," in *2004 IEEE 35th Annual Power Electronics Specialists Conference (IEEE Cat. No. 04CH37551)*, vol. 3. IEEE, 2004, pp. 2054–2059.
- [4] I. S. Mohamed, S. A. Zaid, M. Abu-Elyazeed, and H. M. Elsayed, "Model predictive control-a simple and powerful method to control UPS inverter applications with output LC filter," in *2013 Saudi International Electronics, Communications and Photonics Conference*. IEEE, 2013, pp. 1–6.
- [5] ———, "Classical methods and model predictive control of three-phase inverter with output LC filter for UPS applications," in *2013 International Conference on Control, Decision and Information Technologies (CoDIT)*. IEEE, 2013, pp. 483–488.
- [6] J. Rodriguez and P. Cortes, *Predictive control of power converters and electrical drives*, 1st ed. John Wiley & Sons, 2012.
- [7] S. Kouro, M. Malinowski, K. Gopakumar, J. Pou, L. G. Franquelo, B. Wu, J. Rodriguez, M. A. Pérez, and J. I. Leon, "Recent advances and industrial applications of multilevel converters," *IEEE Transactions on industrial electronics*, vol. 57, no. 8, pp. 2553–2580, 2010.
- [8] S. Kouro, J. Rodriguez, B. Wu, S. Bernet, and M. Perez, "Power the future of industry," *IEEE Trans. Ind. Electron.*, pp. 26–38, 2012.
- [9] J. Rodriguez, S. Bernet, B. Wu, J. O. Ponnt, and S. Kouro, "Multilevel voltage-source-converter topologies for industrial medium-voltage drives," *IEEE Transactions on industrial electronics*, vol. 54, no. 6, pp. 2930–2945, 2007.
- [10] L. G. Franquelo, J. Rodriguez, J. I. Leon, S. Kouro, R. Portillo, and M. A. Prats, "The age of multilevel converters arrives," *IEEE industrial electronics magazine*, vol. 2, no. 2, pp. 28–39, 2008.
- [11] J. Rodriguez, M. P. Kazmierkowski, J. R. Espinoza, P. Zanchetta, H. Abu-Rub, H. A. Young, and C. A. Rojas, "State of the art of finite control set model predictive control in power electronics," *IEEE Transactions on Industrial Informatics*, vol. 9, no. 2, pp. 1003–1016, 2012.
- [12] P. Cortés and J. Rodríguez, "Three-phase inverter with output LC filter using predictive control for UPS applications," in *2007 European Conference on Power Electronics and Applications*. IEEE, 2007, pp. 1–7.
- [13] S. Kwak and J.-C. Park, "Switching strategy based on model predictive control of VSI to obtain high efficiency and balanced loss distribution," *IEEE Transactions on Power Electronics*, vol. 29, no. 9, pp. 4551–4567, 2013.
- [14] I. S. Mohamed, S. A. Zaid, M. Abu-Elyazeed, and H. M. Elsayed, "Improved model predictive control for three-phase inverter with output LC filter," *International Journal of Modelling, Identification and Control*, vol. 23, no. 4, pp. 371–379, 2015.
- [15] F. Defaÿ, A.-M. Llor, and M. Fadel, "Direct control strategy for a four-level three-phase flying-capacitor inverter," *IEEE Transactions on Industrial Electronics*, vol. 57, no. 7, pp. 2240–2248, 2010.
- [16] G. Papafotiou, J. Kley, K. G. Papadopoulos, P. Bohren, and M. Morari, "Model predictive direct torque control—part II: Implementation and experimental evaluation," *IEEE Transactions on industrial electronics*, vol. 56, no. 6, pp. 1906–1915, 2008.
- [17] Z. Song, W. Chen, and C. Xia, "Predictive direct power control for three-phase grid-connected converters without sector information and voltage vector selection," *IEEE Transactions on Power Electronics*, vol. 29, no. 10, pp. 5518–5531, 2013.
- [18] I. S. Mohamed, S. A. Zaid, M. Abu-Elyazeed, and H. M. Elsayed, "Implementation of model predictive control for three-phase inverter with output LC filter on eZdsp F28335 Kit using HIL simulation," *International Journal of Modelling, Identification and Control*, vol. 25, no. 4, pp. 301–312, 2016.
- [19] R. Findeisen, F. Allgöwer, and L. T. Biegler, "Assessment and future directions of nonlinear model predictive control," in *Lecture Notes in Control and Information Sciences*, M. Thomaa and M. Morari, Eds. Springer, 2007, vol. 358, no. 7.
- [20] M. Nauman and A. Hasan, "Efficient implicit model-predictive control of a three-phase inverter with an output LC filter," *IEEE Transactions on Power Electronics*, vol. 31, no. 9, pp. 6075–6078, 2016.
- [21] M. Norambuena, C. Garcia, J. Rodriguez, and P. Lezana, "Finite control set model predictive control reduced computational cost applied to a flying capacitor converter," in *IECON 2017-43rd Annual Conference of the IEEE Industrial Electronics Society*. IEEE, 2017, pp. 4903–4907.
- [22] D. Wang, Z. J. Shen, X. Yin, S. Tang, X. Liu, C. Zhang, J. Wang, J. Rodriguez, and M. Norambuena, "Model predictive control using artificial neural network for power converters," *IEEE Transactions on Industrial Electronics*, 2021.
- [23] S. Kwak, U.-C. Moon, and J.-C. Park, "Predictive-control-based direct power control with an adaptive parameter identification technique for improved AFE performance," *IEEE Transactions on Power Electronics*, vol. 29, no. 11, pp. 6178–6187, 2014.
- [24] C. Martin, M. Bermúdez, F. Barrero, M. R. Arahal, X. Kestelyn, and M. J. Durán, "Sensitivity of predictive controllers to parameter variation in five-phase induction motor drives," *Control Engineering Practice*, vol. 68, pp. 23–31, 2017.
- [25] H. A. Young, M. A. Perez, and J. Rodriguez, "Analysis of finite-control-set model predictive current control with model parameter mismatch in a three-phase inverter," *IEEE Transactions on Industrial Electronics*, vol. 63, no. 5, pp. 3100–3107, 2016.
- [26] B. Bogado, F. Barrero, M. R. Arahal, S. Toral, and E. Levi, "Sensitivity to electrical parameter variations of predictive current control in multiphase drives," in *IECON 2013 39th Annual Conference of the IEEE Industrial Electronics Society*. IEEE, 2013, pp. 5215–5220.
- [27] B. Karanayil and M. F. Rahman, "Artificial neural network applications in power electronics and electrical drives," in *Power Electronics Handbook*. Elsevier, 2011, pp. 1139–1154.
- [28] H. S. Khan, I. S. Mohamed, K. Kauhaniemi, and L. Liu, "Artificial neural network-based voltage control of DC/DC converter for DC microgrid applications," in *2021 6th IEEE Workshop on the Electronic Grid (eGRID)*. IEEE, 2021, pp. 1–6.
- [29] I. S. Mohamed, S. Rovetta, T. D. Do, T. Dragicević, and A. A. Z. Diab, "A neural-network-based model predictive control of three-phase inverter with an output LC filter," *IEEE Access*, vol. 7, pp. 124737–124749, 2019.
- [30] X. Liu, L. Qiu, Y. Fang, Z. Peng, and D. Wang, "Finite-level-state model predictive control for sensorless three-phase four-arm modular multilevel converter," *IEEE Transactions on Power Electronics*, vol. 35, no. 5, pp. 4462–4466, 2019.
- [31] T. Dragicević and M. Novak, "Weighting factor design in model predictive control of power electronic converters: An artificial neural network approach," *IEEE Transactions on Industrial Electronics*, vol. 66, no. 11, pp. 8870–8880, 2018.
- [32] M. T. Wishart and R. G. Harley, "Identification and control of induction machines using artificial neural networks," *IEEE Transactions on Industry Applications*, vol. 31, no. 3, pp. 612–619, 1995.
- [33] H.-Y. Lee, J.-I. Lee, S.-O. Kwon, and S.-W. Lee, "Performance estimation of induction motor using artificial neural network," in *2018 25th International Conference on Systems, Signals and Image Processing (IWSSIP)*. IEEE, 2018, pp. 1–3.
- [34] X. Sun, L. Chen, Z. Yang, and H. Zhu, "Speed-sensorless vector control of a bearingless induction motor with artificial neural network inverse speed observer," *IEEE/ASME Transactions on mechatronics*, vol. 18, no. 4, pp. 1357–1366, 2012.
- [35] A. Baker, M. Alhasheem, and S. Peyghami, "Efficient fixed-switching modulated finite control set-model predictive control based on artificial neural networks," *Applied Sciences*, vol. 12, no. 6, p. 3134, 2022.

- [36] K. Hornik, "Approximation capabilities of multilayer feedforward networks," *Neural networks*, vol. 4, no. 2, pp. 251–257, 1991.
- [37] M. A. Ebrahim, B. A. Aziz, M. N. Nashed, and F. A. Osman, "Optimal design of proportional-resonant controller and its harmonic compensators for grid-integrated renewable energy sources based three-phase voltage source inverters," *IET Generation, Transmission & Distribution*, vol. 15, no. 8, pp. 1371–1386, 2021.
- [38] I. S. Mohamed, "Implementation of model predictive control for three-phase inverter with output LC filter using DSP," Master's thesis, Control Engineering, Faculty of Engineering, Cairo University, 2014.